Title
Spatial and temporal profile of high-frequency oscillations in posttraumatic epileptogenesis.

Authors
Li, Lin
Kumar, Udaya
You, Jing
et al.

Publication Date
2021-12-01

DOI
10.1016/j.nbd.2021.105544

Peer reviewed

HHS Public Access

Author manuscript

Neurobiol Dis. Author manuscript; available in PMC 2022 May 06.

Published in final edited form as:

Neurobiol Dis. 2021 December ; 161: 105544. doi:10.1016/j.nbd.2021.105544.

Spatial and temporal profile of high-frequency oscillations in posttraumatic epileptogenesis

Lin Li[a,b,*,1], **Udaya Kumar**[a,1], **Jing You**[b], **Yufeng Zhou**[b], **Shennan A. Weiss**[c,d], **Jerome Engel**[a,e,f,g], **Anatol Bragin**[a,e,**]

[a]Department of Neurology, University of California Los Angeles, CA 90095, USA

[b]Department of Biomedical Engineering, University of North Texas, TX 76207, USA

[c]Depts. of Neurology, Dept. of Physiology and Pharmacology, State University of New York Downstate, Brooklyn, New York 11203, USA

[d]Department of Neurology, New York City Health + Hospitals/Kings County, Brooklyn, NY 11203, USA

[e]Brain Research Institute, University of California, Los Angeles, CA 90095, USA

[f]Department of Neurobiology, David Geffen School of Medicine at UCLA, Los Angeles, CA 90095, USA

[g]Department of Psychiatry and Biobehavioral Sciences, David Geffen School of Medicine at UCLA, Los Angeles, CA 90095, USA

Abstract

We studied the role of temporal and spatial changes in high-frequency oscillation (HFO, 80–500 Hz) generation in epileptogenesis following traumatic brain injury (TBI).

Experiments were conducted on adult male Sprague Dawley rats. For the TBI group, fluid percussion injury (FPI) on the left sensorimotor area was performed to induce posttraumatic epileptogenesis. For the sham control group, only the craniotomy was performed. After TBI, 8 bipolar micro-electrodes were implanted bilaterally in the prefrontal cortex, perilesional area and homotopic contralateral site, striatum, and hippocampus. Long-term video/local field potential (LFP) recordings were performed for up to 21 weeks to identify and characterize seizures and capture HFOs. The electrode tip locations and the volume of post TBI brain lesions were further estimated by ex-vivo MRI scans. HFOs were detected during slow-wave sleep and categorized

*Correspondence to: L. Li, Department of Biomedical Engineering, University of North Texas, 3940 N.Elm, Denton, TX, USA. lin.li@unt.edu (L. Li). **Correspondence to: A. Bragin, Department of Neurology, University of California Los Angeles, 710 Westwood Plz, Los Angeles, CA 90095, USA. abragin@mednet.ucla.edu (A. Bragin).
[1]These authors contributed equally to this work.

Declaration of Competing Interest

The authors report no competing interests.

We confirm that we have read the Journal's position on issues involved in ethical publication and affirm that this report is consistent with those guidelines.

Appendix A. Supplementary data

Supplementary data to this article can be found online at https://doi.org/10.1016/j.nbd.2021.105544

as ripple (80–200 Hz) and fast ripple (FR, 250–500 Hz) events. HFO rates and the HFO peak frequencies were compared in the 8 recording locations and across 8-weeks following TBI.

Data from 48 rats (8 sham controls and 40 TBI rats) were analyzed. Within the TBI group, 22 rats (55%) developed recurrent spontaneous seizures (E+ group), at an average of 62.2 (+17.1) days, while 18 rats (45%) did not (E− group). We observed that the HFOs in the E+ group had a higher mean peak frequency than the E− group and the sham group ($P < 0.05$). Furthermore, the FR rate of the E+ group showed a significant increase compared to the E−group ($P < 0.01$) and sham control group ($P < 0.01$), specifically in the perilesional area, homotopic contralateral site, bilateral hippocampus, and to a lesser degree bilateral striatum. When compared across time, the increased FR rate in the E+ group occurred immediately after the insult and remained stable across the duration of the experiment. In addition, lesion size was not statistically different in the E+ and E− group and was not correlated with HFO rates.

Our results suggest that TBI results in the formation of a widespread epileptogenic network. FR rates serve as a biomarker of network formation and predict the future development of epilepsy, however FR are not a temporally specific biomarker of TBI sequelae responsible for epileptogenesis. These results suggest that in patients, future risk of post-TBI epilepsy can be predicted early using FR.

Keywords

Ripple; Fast ripple; Extrahippocampal HFO; Posttraumatic epilepsy; Epileptogenesis

1. Introduction

High-frequency oscillations (HFOs) are brief (15–300 msec) bursts of high-frequency energy in the electroencephalogram (EEG), or local field potentials (LFP), with a spectral content between 80 and 500 Hz (Buzsaki et al., 1992). HFOs can be further classified as ripples (80–200 Hz) and fast ripples (FR, 250–500 Hz). In patients with medically refractory epilepsy, rates of ripples and FRs are increased in the SOZ (Jacobs et al., 2008; Ferrari-Marinho et al., 2016; Perucca et al., 2014), and failure to resect brain regions with elevated ripple and FR rates correlates with a non-seizure free outcome following epilepsy surgery (Fedele et al., 2017; Modur et al., 2011). Thus, HFOs may be a biomarker of the epileptogenic zone (EZ) which is the region necessary and sufficient for seizure generation (Rěhulka et al., 2019; Zijlmans et al., 2012; Worrell et al., 2004; Frauscher et al., 2017). FRs, which occur less often then ripples, have been shown to be a more specific biomarker of the EZ and better correlate with poor outcome if left unresected (Bragin et al., 2002a; Bragin et al., 2003; Wu et al., 2010).

In animal models of epilepsy, fast ripples appear to be a biomarker of epileptogenesis. In the kainic acid model, following intra-hippocampal injection, FRs are significantly increased in the hippocampus and entorhinal cortex ipsilateral to the injection site, while ripple rates are increased bilaterally (Bragin et al., 1999). In animal models of PTE, repetitive high-frequency oscillations with spikes (rHFOSs) were reported to occur in the perilesional areas after lateral fluid percussion injury and rHFOSs displayed higher occurrence rates

in the early period compared to the late period (Reid et al., 2016). FRs are believed to be generated by synchronized action potentials produced by small clusters (<1 mm^3) of pathologically inter connected neurons (PIN-clusters) (Bragin et al., 2003; Bragin et al., 2000). It has been hypothesized that these PIN clusters participate in epileptogenesis by producing interictal events that can directly trigger seizures[12]. Notably, following kainic acid injection, FR rates increase rapidly and dramatically, suggesting that they are temporally specific biomarkers of the epileptogenic changes in the network (Bragin et al., 2004; Bragin et al., 2002b).

Epileptogenesis that follows TBI may require years before the first seizure (Pitkänen and Immonen, 2014). It is thought that this process involves excitotoxicity, neuroinflammation, oxidative stress, apoptosis, and neuronal plasticity (Pitkanen et al., 2015; Pitkanen et al., 2016; Bertoglio et al., 2019; Chauviere et al., 2012). The latent period between brain insult and symptomatic epilepsy is an important time window for investigation of pathophysiological changes taking place in the brain in order to understand mechanisms of formation of pathological networks. Since FRs have served as temporally and spatially specific biomarkers of epileptogenesis in other animal models of epilepsy (Bragin et al., 2004; Bragin et al., 2002b; Jiruska et al., 2010), we hypothesized that FRs would serve similarly in TBI induced epilepsy. To study posttraumatic epilepsy, we used the fluid percussion injury (FPI) rat model because it is reliable and can reproduce many important features in brain injury observed in other models and species (Dixon et al., 1987; Kabadi et al., 2010). We compared HFO rates in sham animals, TBI treated animals without seizures, and TBI treated animals with seizures. To investigate the spatial dynamics of HFOs we recorded LFPs from the prefrontal cortex, striatum, and perilesional sites, along with hippocampus bilaterally. We preformed these recordings over an eight-week duration to measure the temporal dynamics. Finally, to test the hypothesis that lesion severity correlates with epileptogenesis we performed ex-vivo structural MRI and compared lesion volume to HFO rates.

2. Materials and methods

2.1. Experimental protocols

Sixty-nine adult Sprague-Dawley (300–350 g) male rats were used in this study. Fifty-nine animals received the TBI protocol, and ten severed as sham control and received only a craniotomy. TBI was induced using the FPI general procedure (Giza et al., 2002; Prins et al., 1996; Bragin et al., 2016) developed at UCLA department of neurosurgery. The animals were first anesthetized with isoflurane (4–5% for induction, 1.5–2% for maintenance). Then the flunixin meglumine (2.5 mg/kg) was administered intravenouslyand lidocaine (2%) was applied subcutaneously to the skull. The skull was then exposed and cleaned with sterile saline, and a 5.0 mm diameter craniotomy was performed over the left sensorimotor cortex, centered 3.0 mm posterior to the bregma, 6.0 mm lateral to the midline. An injury cap (5.0 mm inner diameter, made from a 1 ml syringe barrel) was glued outside the craniotomy edge above the skull and fixed with dental cement. As guided by our previous published work (Giza et al., 2002; Prins et al., 1996; Bragin et al., 2016), the percussion intensity at 3.2 to 3.5 atm percussion force was applied from the custom-made pneumatic

device. Specifically, the isoflurane anesthesia was discontinued and FPI was induced after the animal wasres-ponsive to toe pinch. Following TBI or sham injury, the animals were kept on the heating pad which was maintained at 37 ○C until the first response to toe pinch. The rats were then implanted with eight bipolar depth electrodes (see Section 2.2). Following implantation, long-term non-continuous video-LFP recordings was performed for 8–21 weeks (Fig. 1. A). The experiments were stopped depending on the animal's health conditions, seizure occurrence, and recording cap conditions. Following VLFP monitoring, the animals were perfused and the brains were imaged using a Bruker Biospin 7 Tesla scanner at the University of California Los Angeles (UCLA) Brain Mapping Center to verify the electrode placement and estimate the volume of the brain lesion (Supplementary materials). Twenty-two animals were excluded due to either poor recordings, or electrode displacement. This experimental protocol was approved by the Institute Animal Care and Use Committee (IACUC) of UCLA (protocol number 2000–153–61A).

2.2. Electrode implantation and electrophysiological data acquisition

Eight bipolar 50-μm diameter tungsten microelectrodes with 1 mm space separation between the tips were used for intracranial LFP recordings. The bipolar electrodes were implanted into 4 brain areas bilaterally (Fig. 1B&C): prefrontal cortex (L/RFC, coordinates (in millimeters), anterior-posterior [AP] = 3.7, medial-lateral [ML] =+/ −0.5, dorsal-ventral [DV] = 3.0), striatum (L/RST, [AP] = 1.6, [ML] = ±1.8, [VD] = 6.0), TBI core ([AP] = −5.0, [ML] = 3.0, [VD] = 1.0), contralateral TBI core (L/RTBI, [AP] −5.0, [ML] 3.0, [VD] 1.0), and hippocampus (L/RHP, [AP] = −5.2, [ML] = ±5.2, [VD] = 7.4 (Paxinos and Watson, 2009)). The ground and reference electrodes (stainless steel screws) were placed in the cerebellum, 2.0 mm posterior to lambda and 1.0 mm lateral from the sagittal suture.

Recordings were performed in a reduced light chamber (Tecniplast, USA), and animals were monitored using an infrared video camera at 30 frames per second. The LFPs were amplified using a 16-channel wide-bandwidth IntanTech amplifier (California, USA) at a sampling rate of 3 kHz. Data acquisition was performed using Intan Data Acquisition software and data was saved in 10-bit binary format for subsequent review and analysis. Time-locked video-LFP recordings began within an hour after electrode implantation. LFP was recorded 10–12 h per day. Video recording was performed continuously 24 h/day before the animal was perfused. The length of the video-LFP recording in animals varied from a minimum of 2 months to 21 weeks (149 days) depending on the time till first seizure, or the time of electrode displacement.

2.3. Data analysis

2.3.1. Estimation of post TBI brain injury—TBI related brain lesion volume was determined by ex-vivo MRI in 8 rats from the E-group and 12 rats from the E+ group. The post TBI brain injury lesion volume (mm^3) was measured by the approach described by Turtzo et al. (Turtzo et al., 2013) by first stripping the brain using an automatic brain extraction tool (https://fsl.fmrib.ox.ac.uk/fsl/fslwiki/BET (Smith, 2002; Jenkinson et al., 2005)), and then using a segmentation algorithm (Zhang et al., 2001) (FSL-FAST https://fsl.fmrib.ox.ac.uk/fsl/fslwiki/FAST) applied to the T2-weighted MRI of the post-brain injury cortex to automatically mask the lesion areas. The lesion volumes were further quantified

based on the segmented data and were further confirmed by two experts (Bragin & Li). Cyst formations from the TBI were excluded.

2.3.2. Seizure detection—LFP recordings were converted to European Data Format (EDF) (Kemp et al., 1992) for visual review in the EDF browser (https://www.teuniz.net/edfbrowser/). Seizures were defined as ictal paroxysmal electrical activity with amplitude 3 times higher than the mean amplitude lasting >10 s, with or without behavioral correlates estimated by time-locked video recordings.

2.3.3. Automatic detection of HFOs—For each animal, a 1–2 h LFP recording epoch containing visually identified slow wave sleep (Grosmark et al., 2012) was randomly selected during one day each week for the first 8 weeks of the experiment. The selected periods were concatenated in one 1–2 h file, removing an amplitude gaps between the fragments. HFOs were then detected using an automatic two-step algorithm implemented in Matlab version 2019b (Natick, MA, see supplementary materials for details). In brief, to identify ripple and fast ripple events efficiently, a Staba root-mean square energy detector was used (Staba et al., 2002), and several time-frequency features such as mean and total power of the contour, onset and offset, and total weighted frequency were used to build the comprehensive classification pipeline (Waldman et al., 2018). The ripple and fast ripple rates (num/min) were quantified with respect to spatial (brain regions) and the temporal distribution (weekly).

2.4. Statistical analysis

2.4.1. Analysis of HFO occurrence rates—Statistical analysis was performed using GraphPad Prism 8 (GraphPad Software) or MATLAB 2019b. For the HFO data, the Ripple and FR rates were computed per brain region per week period. We have identified three main effects, including “group” – 3 levels: control, E− and E+; “area” – 8 levels: L/RFC, L/RST, L/RTBI and L/RHP; “period” – 8 levels: week1 through week8. In this study, we were specifically interested to study the “group” factor in response to the ripple and FR occurrence rates, as well as the “group area” and “group period” interactions. In addition, for the with-group comparisons, a separate analysis was performed by assuming that the “area” and “period” factors were independent. The Kolmogorov-Smironov test was applied to test the normality of the data. For the normally distributed data, the repeated-measures ANOVA was used. Specifically, in the brain area analysis, the Two-Way Repeated-Measures ANOVA compared the event rate (num/min) in different groups (control, E− and E+) across four regions (prefrontal, striatum, perilesion, hippocampus). In the time analysis, the same analysis was performed but compared the recording periods (week 1 to week 8). A multicomparison (Tukey corrected) were applied to estimate the group differences of total HFO, ripple, and FR rates. For data that failed the normality test, Mann-Whitney or Wilcoxon tests were applied. An alpha level of 0.05 was used in hypothesis test.

2.4.2. Estimation of TBI related brain damage—To compare post-TBI brain lesion volumes between groups the two-sample *t*-test was performed. Since the lesion volume data were not normally distributed, a bootstrapping analysis (Yung and Bentler, 1996) was implemented using 1000 surrogates. Bootstrapping estimation of lesion size was computed

on each group independently. The outcome stability was estimated through the "central tendency" distribution. The group difference was estimated by the 95% confidence of interval (CI) of the bootstrapping distribution.

2.4.3. Validation of the temporal stability and result reliability of ripple and FR occurrences—The temporal stability of ripple and fast ripple rates within each group was estimated by the intraclass correlation coefficient (ICC) (Koo and Li, 2016; Li et al., 2015), combined with the column and row adjusted random imputation (CRARI (Courrieu and Rey, 2011)). The weekly ripple and fast ripple rates were tested within groups and the event rate reliability was reported followed by the criteria suggested in (Koo and Li, 2016): a ICC value <0.5 are indicative of poor reliability, value between 0.5 and 0.75 indicate moderate reliability, values between 0.75 and 0.9 indicate good reliability, and values greater than 0.90 indicate excellent reliability. Alternatively, bootstrapping distributions (surrogates = 1000) were further computed on the weekly ripple rate and fast ripple rate within each group to estimate the result reliability. The weekly ripple and fast ripple rate distributions within each group was computed and stacked within each group. The within-group weekly HFO rate consistency was verified by comparing the 95%CI on bootstrapping distribution across each week.

2.5. Data availability

The data that support the findings of this study are available from the authors upon reasonable request.

3. Results

3.1. The measurements of the HFOs during posttraumatic epileptogenesis

In our study, 22 out of 40 TBI-treated rats developed recurrent seizures and were classified as E+ (n = 22). The rest of the TBI-treated animals (n = 18) showed no signs of electrophysiological and/or behavioral seizures during the experimental periods (up to 21 weeks, or 149 days), and were categorized as E−. The average first recurrent seizure in the E+ rats occurred at 62.2 (±17.1) days (see Fig. 1D and Supplementary Table S1). None of the sham control rats (n = 10) developed seizures.

From the E+, E−, and sham control animals, a total of 203,550 HFOs, including 150,874 ripple events and 52,676 fast ripple events were isolated (Table 1). Of these HFOs, 133,070 HFO events were detected in the E+ group (3.64 ± 3.49/min), 53,622 were found in the E− group (1.82 ± 2.22/min) and 16,858 were found in the sham group (1.00 ± 1.32/min). Prior to analyzing HFO rates across the groups, we first examined differences in HFO mean peak frequency. Mean HFO peak frequency was compared at the level of pooled events across the experiment duration and across rats within each group (Fig. 2A). The mean HFO peak frequency in the E+ group was significantly faster than both the E− and the sham group ($p < 0.01$), but there was no difference between the mean peak frequency of the sham and E− group ($p = 0.14$). Within groups, and across the experimental duration of 8 week testing periods, we found no difference in the HFO peak frequency (control: $p = 0.13$; E−: $p = 0.72$; E+: $p = 0.06$) (Fig. 2C).

To examined changes in HFO rates following TBI we first distinguished ripples from fast ripples (FR), on the basis of event frequency. Differences in ripple and FR rates were computed for the sham, E−, and E+ groups, for the 8 sampled neuroanatomic regions, and for the eight weekly recording epochs using a 3-way ANOVA (Fig. 3A&B). This analysis revealed that ripple and FR rates were significantly different for the E+, E− and sham groups, (Ripple, $p = 0.03$; FR, $p < 0.001$); the ripple and FR rates were also different for the eight neuroanatomic region sampled by the electrodes, (Ripple, $p < 0.001$; FR, $p = 0.02$); however, the rate of ripples and FRs was not statistically different for the different recording epochs across the experimental duration (Ripple, $p = 0.13$; FR, $p = 0.31$) (Supplementary Fig. S1). Pooling across all the neuroanatomical recording sites and time, we found significant differences for E+ > control ($p = 0.012$) in ripple rates (Fig. 3C), and E+ > E− ($p = 0.002$) and E+ > control ($p = 0.004$) in FR rates (Fig. 3D).

3.2. Spatial distribution of HFO occurrence in posttraumatic epileptogenesis

To determine whether HFO rates ipsilateral to the TBI differed from contralateral sites we pooled HFO rates derived from the ipsilateral recording sites across time and within groups. The HFO rates were compared to test within- and between-groups. The ripple rate showed no differences between ipsilateral and contralateral side within all three groups [two-way ANOVA, $F(1, 90) = 0.15$, $p = 0.69$)] (Fig. 4A). FR rates also showed no differences between the ipsilateral and contralateral side [two-way ANOVA, $F(1, 90) = 0.38$, $p = 0.54$] (Fig. 4B). While no differences were found when comparing rates across all recording sites, between-group differences of ripple rates in ipsilateral and contralateral side were found in E vs. control (E > control, $p = 0.015$). In addition, the E+ group revealed the highest FR rates compared to the E− ($p < 0.001$) and control ($p < 0.001$) groups. No differences were found between E− and control groups in both ripple and FR rates ($p = 0.53$) (Fig. 4A&B and Supplemental Table S2).

Ripple and FR rates were further compared to estimate group-difference in the four recording sites individually: the bilateral prefrontal cortex, striatum, perilesional site, and hippocampus. The E+ group showed an elevated ripple rate only in the perilesional sites and homotopic contralateral sites (E+ > E−, $p = 0.006$, E+ > sham, $p = 0.006$) and bilateral hippocampi (E+ > E−, $p = 0.02$, E+ > sham, $p = 0.001$), compared to the E− and control groups (Fig. 4C). The FR rates were also elevated in the perilesional sites, the homotopic contralateral sites, and bilateral hippocampi in the E+ group compared to the E− group (perilesional: E+ > E−, $p < 0.001$; hippocampus: E+ > E−, $p < 0.001$). Additionally, FR rates were also elevated in the bilateral striatum when comparing E+ to the control group (perilesional: E+ > control, $p < 0.001$; E+ > control, $p < 0.001$; striatum: E+ > control ($p = 0.035$) (Fig. 4D, Supplementary Table S3).

3.3. Temporal changes in HFO rate following TBI

To better understand changes in HFO rate from week 1 to week 8 after the TBI procedure, the within-group HFO rate differences were estimated by comparing average ripple and FR rates of each week, to week 1, in each group. There were no significant differences for within-group ripple rates [two-way ANOVA, $F(7, 360) = 0.22$, $p = 0.98$] and FR rates [two-way ANOVA, $F(7, 360) = 0.071$, $p = 0.99$], across the experimental duration, in either

the E+ or E− group (Fig. 5A&B). To better test for HFO rate stability across the experiment duration, we calculated corrected intraclass correlation coefficients (rICCs) for HFO rates. rICCs showed a good-to-excellent reliability of weekly ripple rates in all groups (control = 0.73, E− = 0.94, E+ = 0.73). Similar results were obtained for the weekly FR rates (control = 0.81, E− = 0.91, E+ = 0.77) (Fig. 5C&D). Furthermore, we used a bootstrapping method and found no significant differences for each of the three groups ($p > 0.05$, Fig. 5E&F).

To determine when epileptogenic changes occurred after the TBI, we compared ripple and FR rates between the groups during each of the 8 weeks using a two-way ANOVA (Supplementary Table S4). Between-group differences for ripple rate were evident (two-way ANOVA, F (2,360) = 16, $p < 0.001$). Subgroup analysis revealed no differences in ripple rates between E− and sham groups across the experimental duration. However, ripple rates in the E+ group were greater than sham in week 2 ($p = 0.044$), week 5 ($p = 0.019$), week 6 ($p = 0.044$), week 7 ($p = 0.045$), and week8 ($p = 0.027$). The ripple rates were greater in E+ vs. E− group only in week 5 ($p = 0.014$), which may have been an anomaly because this increase did not persist. (Fig. 5A). In contrast, when we examined FR rates we found that the E+ group had significantly greater FR rates across all eight weeks compared to both E− and control groups (two-way ANOVA, F(2, 360) = 48, $p < 0.001$, Fig. 5B). No FR rate difference were observed between the E− and control groups across the experimental duration. In addition, we applied a bootstrapping analysis (nboot = 1000) and confirmed the consistent findings by comparing the bootstrapping distribution with the post-hoc analysis, indicating a high result reliability (Supplementary Fig. S2).

3.4. Relationship of lesion size and the occurrence of HFO

We further investigated the relationship between the volume of the brain lesion (mm^3) in the TBI-treated animals (E−, n = 8 and E+ group, n = 12) and the corresponding rates of HFOs using a linear regression analysis. The average lesion volume of the E+ and E− groups was 14.44 ± 1.38 mm^3 and 13.86 ± 1.87 mm^3, respectively. No significant differences in lesion size ($p = 0.80$) were found between the two groups (Fig. 6A). The reliability of this result was further confirmed using bootstrapping (surrogates = 1000, Fig. 5A). For the linear regression analysis comparing HFO rates to lesion volume, ripple rates and FR rates were analyzed independently in the E+ group (Fig. 6B&C) and the E− group (Fig. 6D&E). We found no significant correlation between HFO rates and lesion volume in the E+ group ($R^2 = 0.0016$, $p = 0.89$ for ripples; $R^2 = 1.23 \times 10^{-5}$, $p = 0.99$ for FR). In addition, there was no linear relationship between HFO rates and lesion volume in the E− group ($R^2 = 0.17$, $p = 0.31$ for ripples; $R^2 = 0.048$, $p = 0.60$ for FR).

4. Discussion

This study is the first to investigate the spatial-temporal evolution of HFO generation during epileptogenesis in a rodent model of post-traumatic epilepsy. We were able to reliably phenotype the rats into control, E− and E+ groups based on electroclinical diagnosis. We then used a HFO detection algorithm to characterize a quarter million HFO events weekly across the eight-week period from four bilateral brain regions that may be involved in epileptogenesis. We observed the following primary findings after TBI: (1) E+ animals

stably generate HFOs with a faster mean peak frequency content than E− or control animals; (2) Overall, FR but not ripple rates were increased in the E+ group, but not the E− group or sham group; (3) HFOs were increased both ipsilateral and contralateral to the lesion; (4) HFO rate differences between the E+ group and E− group were most significant in the perilesional site, the homotopic contralateral site, and bilateral hippocampi; (5) The increase in FR rate in the E+ group compared to the E− group was stable across the experimental duration (4) The volume of the lesion did not differ in the E+ and the E− group and was nor correlated with the ripple or FR rates.

4.1. Justification of the experimental designs

The time course of TBI induced epileptogenesis demonstrated in our experiments is consistent with prior results from our laboratory (Reid et al., 2016; Bragin et al., 2016), the first spontaneous seizure was observed at an average of day 62.2 (±17.1), with the earliest onset at day 36 and latest at day 88. Video-LFP data was recorded for up to 149 days. Fitting a gamma distribution, we can estimate a 126 day period in order to reach a 99% probability of knowing whether an animal will become E+ or not. We selected only the first 8-weeks of electrophysiological data for analysis to maintain a reasonable sample pool to capture the early events associated with epileptogenesis. Since we found stable HFO rates across the experimental duration, it is unlikely that extending the observation period would have dramatically changed the results.

4.2. Spatial-temporal distributions of HFOs in epileptogenesis

Both ripples and FRs showed significant differences between E+ group and E−/control group in the perilesional site, homotopic contralateral site, and bilateral hippocampus, which were the sites of seizure onset for most E+ rats (data not provided). This result is consistent with prior studies which found that FR rates are increased in the SOZ and EZ (Worrell et al., 2004; Wu et al., 2010; Staba et al., 2002; González Otárula et al., 2018). However, we also found that HFO rates were increased both ipsilateral and contralateral to the lesion indicating a more widespread pattern of HFO generation after TBI. Prior investigators using either pharmacologic approaches or TBI to induce epileptogenesis have also found that a unilateral lesion results in bilateral seizures and interictal HFOs (Bragin et al., 2003; Sheybani et al., 2018; Li et al., 2018). Our results reconfirm these findings and also suggest that subcortical structures may be involved, since we found differences in FR rates in the striatum between the E+ and E− groups. Overall, our results are consistent with the network hypothesis, that seizure generation requires the interplay of multiple potentially epileptogenic brain regions, and that following an insult the involved epileptogenic brain regions can be diverse and spatially distant (Li et al., 2021; Bullmore and Sporns, 2009).

With respect to changes in HFO generation over the duration of the experiment, the longitudinal data revealed that as early as the first week, the FR rates were elevated in the E+ group compared to the E− and control groups. The FR rates in the E+ group remained stably elevated across the 8-week experimental duration. This finding suggests that following TBI, the FR rates can reliably predict the future development of seizures. This is similar to what we observed in the KA model of epileptogenesis (Bragin et al., 1999). Based on these data we can suggest that the neuronal substrates responsible for epileptogenesis are similar in

both models of epilepsy, KA and TBI, and may depend on the formation of networks of PIN-clusters (Bragin et al., 2000). In summary, the increase in FR following TBI appears to serves as a predictive biomarker of future seizures, but does not dynamically track changes associated with TBI induced epileptogenesis. Future work is needed to better understand the neurophysiological mechanisms responsible for FR generation after TBI and how these relate to post-TBI brain changes.

4.3. No relationship of lesion size with epileptogenesis

There were no differences of the lesion volumes between the E− and E+ animals. While some studies using penetrating brain injury have found a correlation between lesion volume and the development of PTE (Kendirli et al., 2014), other studies using FPI have not (Manninen et al., 2020). In the clinical literature, the risk of developing post-traumatic epilepsy is thought to be highly dependent on injury severity (Frey, 2003). Again, the severity measurement of TBI usually differs among studies, besides MRI based lesion volume measurements of the focal lesion, other methods can capture diffuse lesions through diffusion tensor magnetic-resonance imaging (DTI), which characterizes the three-dimensional spatial distribution of water diffusion in each voxel since the direction of water diffusion reflects the direction of the nerve tracts. (Benson et al., 2007; Basser and Pierpaoli, 2011). Further research is needed to explain this disparity between animal models of TBI and TBI in patients, involving additional methods to quantify TBI severity.

4.4. Study limitations

The accuracy of our results was limited by our ability to classify subjects as E+ and E−. We used 24 h video and 12 h a day Video-LFP recordings to attempt to identify seizures in the subjects. Admittedly because of both subtle clinical seizures, and only half day electrographic recordings, some seizures may have been missed. Because the E+ animals were classified as experiencing recurrent seizures, the likelihood of repeatedly missing events is reduced. However, with the current approach for identification of seizures, we admit that the percentage of animals in the E− group may be an overestimate. Since some E− subjects should in fact be E+ subjects if their seizures had not been missed.

Another shortcoming of this study is that we did not examine the correlation between HFO rates and seizure frequency and severity in out TBI model and experiments. This important issue could be addressed in subsequent experiments.

5. Conclusion

Using the FPI model to induce TBI we found that, exclusively in animals that developed seizures, FR rates are significantly elevated in cortical and subcortical bilateral brain regions immediately following the insult. This increase in FR rates was not correlated with the volume of the lesion and remained stable across the 8-week duration of the experiment. Our results are consistent with the notion that TBI results in a widespread pathologically interconnected epileptogenic networks during the latent period of epileptogenesis. While FR rates were predictive of future seizures, they were stable over time suggesting that they do not serve as a temporally specific biomarker of epileptogenic mechanisms that follow

the initial insult. Fast ripples are thought to be generated by synchronized action potentials from pathologically interconnected neuronal clusters (Bragin et al., 2000). Future work should focus on understanding the mechanisms by which these clusters develop immediately following the injury and remain stable over the sequelae of the injury. It is also unclear why lesion volume did not correlate with fast ripple rates. An important implication of this study is that, since FR can be recorded from the scalp (Pizzo et al., 2016), especially reliable in children (Bernardo et al., 2020), FR may provide a clinically useful tool to identify TBI patients who will develop post traumatic epilepsy

Supplementary Material

Refer to Web version on PubMed Central for supplementary material.

Acknowledgments

Funding

This study was supported by National Institutes of Health, USA R01-NS065877 and R56-NS065877 (A.B), R01-NS033310 (J.E), U54-NS100064 (J.E), and University of North Texas Faculty Research Award 1600733 (L.L).

Abbreviations:

HFOs	High-frequency oscillations
LFP	Local field potential
EZ	Epileptogenic zone
rHFOSs	High-frequency oscillations with spikes
PIN-cluster	Pathologically inter connected neuron
SOZ	Seizure onset zone
FPI	Fluid percussion injury
EDF	European Data Format
ICC	Intraclass correlation coefficient
CRARI	Column and row adjusted random imputation
UCLA	University of California Los Angeles

References

Basser PJ, Pierpaoli C, 2011. Microstructural and physiological features of tissues elucidated by quantitative-diffusion-tensor MRI. J. Magn. Reson. 213 (2), 560–570. [PubMed: 22152371]

Benson RR, Meda SA, Vasudevan S, Kou Z, Govindarajan KA, Hanks RA, et al. , 2007. Global white matter analysis of diffusion tensor images is predictive of injury severity in traumatic brain injury. J. Neurotrauma 24 (3), 446–459. [PubMed: 17402851]

Bernardo D, Nariai H, Hussain SA, Sankar R, Wu JY, 2020. Interictal scalp fast ripple occurrence and high frequency oscillation slow wave coupling in epileptic spasms. Clin. Neurophysiol. 131 (7), 1433–1443. [PubMed: 32387963]

Bertoglio D, Jonckers E, Ali I, Verhoye M, Van der Linden A, Dedeurwaerdere S, 2019. In vivo measurement of brain network connectivity reflects progression and intrinsic disease severity in a model of temporal lobe epilepsy. Neurobiol. Dis. 127, 45–52. [PubMed: 30798008]

Bragin A, Engel J, Wilson CL, Fried I, Mathern GW, 1999. Hippocampal and entorhinal cortex high-frequency oscillations (100–500 Hz) in human epileptic brain and in Kainic acid-treated rats with chronic seizures. Epilepsia. 40 (2), 127–137. [PubMed: 9952257]

Bragin A, Wilson CL, Engel J, 2000. Chronic epileptogenesis requires development of a network of pathologically interconnected neuron clusters: a hypothesis. Epilepsia.41 (s6), S144–S152. [PubMed: 10999536]

Bragin A, Mody I, Wilson CL, Engel J, 2002a. Local generation of fast ripples in epileptic brain. J. Neurosci. 22 (5), 2012–2021. [PubMed: 11880532]

Bragin A, Wilson CL, Staba RJ, Reddick M, Fried I, Engel J, 2002b. Interictal high-frequency oscillations (80–500Hz) in the human epileptic brain: entorhinal cortex. Ann. Neurol. 52 (4), 407–415. [PubMed: 12325068]

Bragin A, Wilson CL, Engel J, 2003. Spatial stability over time of brain areas generating fast ripples in the epileptic rat. Epilepsia. 44 (9), 1233–1237. [PubMed: 12919396]

Bragin A, Wilson CL, Almajano J, Mody I, Engel J, 2004. High-frequency oscillations after status epilepticus: epileptogenesis and seizure genesis. Epilepsia. 45 (9), 1017–1023. [PubMed: 15329064]

Bragin A, Li L, Almajano J, Alvarado-Rojas C, Reid AY, Staba RJ, et al. , 2016. Pathologic electrographic changes after experimental traumatic brain injury. Epilepsia. 57 (5), 735–745. [PubMed: 27012461]

Bullmore E, Sporns O, 2009. Complex brain networks: graph theoretical analysis of structural and functional systems. Nat. Rev. Neurosci. 10 (3), 186–198. [PubMed: 19190637]

Buzsaki G, Horvath Z, Urioste R, Hetke J, Wise K, 1992. High-frequency network oscillation in the hippocampus. Science 256 (5059), 1025–1027. [PubMed: 1589772]

Chauviere L, Doublet T, Ghestem A, Siyoucef SS, Wendling F, Huys R, et al. , 2012. Changes in interictal spike features precede the onset of temporal lobe epilepsy. Ann. Neurol. 71 (6), 805–814. [PubMed: 22718546]

Courrieu P, Rey A, 2011. Missing data imputation and corrected statistics for large-scale behavioral databases. Behav. Res. Methods 43 (2), 310–330. [PubMed: 21424187]

Dixon CE, Lyeth BG, Povlishock JT, Findling RL, Hamm RJ, Marmarou A, et al. , 1987. A fluid percussion model of experimental brain injury in the rat. J. Neurosurg. 67 (1), 110–119. [PubMed: 3598659]

Fedele T, Burnos S, Boran E, Krayenbühl N, Hilfiker P, Grunwald T, et al. , 2017. Resection of high frequency oscillations predicts seizure outcome in the individual patient. Sci. Rep. 7 (1).

Ferrari-Marinho T, Perucca P, Dubeau F, Gotman J, 2016. Intracranial EEG seizure onset-patterns correlate with high-frequency oscillations in patients with drug-resistant epilepsy. Epilepsy Res. 127, 200–206. [PubMed: 27635628]

Frauscher B, Bartolomei F, Kobayashi K, Cimbalnik J, Van't Klooster MA, Rampp S, et al. , 2017. High-frequency oscillations: the state of clinical research. Epilepsia 58 (8), 1316–1329. [PubMed: 28666056]

Frey LC, 2003. Epidemiology of posttraumatic epilepsy: a critical review. Epilepsia. 44 (s10), 11–17.

Giza CC, Prins ML, Hovda DA, Herschman HR, Feldman JD, 2002. Genes preferentially induced by depolarization after concussive brain injury: effects of age and injury severity. J. Neurotrauma 19 (4), 387–402. [PubMed: 11990346]

González Otárula KA, Khoo HM, Von Ellenrieder N, Hall JA, Dubeau F, Gotman J, 2018. Spike-related haemodynamic responses overlap with high frequency oscillations in patients with focal epilepsy. Brain. 141 (3), 731–743. [PubMed: 29360943]

Grosmark AD, Mizuseki K, Pastalkova E, Diba K, Buzsaki G, 2012. REM sleep reorganizes hippocampal excitability. Neuron. 75 (6), 1001–1007. [PubMed: 22998869]

Jacobs J, Levan P, Chander R, Hall J, Dubeau F, Gotman J, 2008. Interictal high-frequency oscillations (80–500 Hz) are an indicator of seizure onset areas independent of spikes in the human epileptic brain. Epilepsia 49 (11), 1893–1907. [PubMed: 18479382]

Jenkinson M, Pechaud M, Smith S, 2005. BET2: MR-based estimation of brain, skull and scalp surfaces. In: Eleventh Annual Meeting of the Organization for Human Brain Mapping. Toronto.

Jiruska P, Finnerty GT, Powell AD, Lofti N, Cmejla R, Jefferys JG, 2010. Epileptic high-frequency network activity in a model of non-lesional temporal lobe epilepsy. Brain. 133 (5), 1380–1390. [PubMed: 20400525]

Kabadi SV, Hilton GD, Stoica BA, Zapple DN, Faden AI, 2010. Fluid-percussion–induced traumatic brain injury model in rats. Nat. Protoc. 5 (9), 1552–1563. [PubMed: 20725070]

Kemp B, Varri A, Rosa AC, Nielsen KD, Gade J, 1992. A simple format for exchange of digitized polygraphic recordings. Electroencephalogr. Clin. Neurophysiol. 82 (5), 391–393. [PubMed: 1374708]

Kendirli MT, Rose DT, Bertram EH, 2014. A model of posttraumatic epilepsy after penetrating brain injuries: effect of lesion size and metal fragments. Epilepsia. 55 (12), 1969–1977. [PubMed: 25470332]

Koo TK, Li MY, 2016. A guideline of selecting and reporting intraclass correlation coefficients for reliability research. J. Chiropract. Med. 15 (2), 155–163.

Li L, Zeng L, Lin Z-J, Cazzell M, Liu H, 2015. Tutorial on use of intraclass correlation coefficients for assessing intertest reliability and its application in functional near-infrared spectroscopy–based brain imaging. J. Biomed. Opt. 20 (5), 050801.

Li L, Patel M, Almajano J, Engel J, Bragin A, 2018. Extrahippocampal high-frequency oscillations during epileptogenesis. Epilepsia. 59 (4), e51–e55. [PubMed: 29508901]

Li L, He L, Harris N, Zhou Y, Engel J Jr., Bragin A, 2021. Topographical reorganization of brain functional connectivity during an early period of epileptogenesis. Epilepsia 62 (5), 1231–1243. 10.1111/epi.16863. [PubMed: 33720411]

Manninen E, Chary K, Lapinlampi N, Andrade P, Paananen T, Sierra A, et al. , 2020. Early increase in cortical T2 relaxation is a prognostic biomarker for the evolution of severe cortical damage, but not for epileptogenesis, after experimental traumatic brain injury. J. Neurotrauma 37 (23), 2580–2594. [PubMed: 32349620]

Modur PN, Zhang S, Vitaz TW, 2011. Ictal high-frequency oscillations in neocortical epilepsy: implications for seizure localization and surgical resection. Epilepsia. 52 (10), 1792–1801. [PubMed: 21762451]

Paxinos G, Watson C, 2009. The Rat Brain in Stereotaxic Coordinates: Compact Sixth Edition. Academic Press, New York.

Perucca P, Dubeau F, Gotman J, 2014. Intracranial electroencephalographic seizure- onset patterns: effect of underlying pathology. Brain 137 (1), 183–196. [PubMed: 24176980]

Pitkänen A, Immonen R, 2014. Epilepsy related to traumatic brain injury. Neurotherapeutics. 11 (2), 286–296. [PubMed: 24554454]

Pitkanen A, Lukasiuk K, Dudek FE, Staley KJ, 2015. Epileptogenesis. Cold Spring Harb Perspect Med. 5 (10).

Pitkanen A, Loscher W, Vezzani A, Becker AJ, Simonato M, Lukasiuk K, et al. , 2016. Advances in the development of biomarkers for epilepsy. Lancet Neurol. 15 (8), 843–856. [PubMed: 27302363]

Pizzo F, Frauscher B, Ferrari-Marinho T, Amiri M, Dubeau F, Gotman J, 2016. Detectability of fast ripples (>250 Hz) on the scalp EEG: a proof-of-principle study with subdermal electrodes. Brain Topogr. 29 (3), 358–367. [PubMed: 26920404]

Prins ML, Lee SM, Cheng CL, Becker DP, Hovda DA, 1996. Fluid percussion brain injury in the developing and adult rat: a comparative study of mortality, morphology, intracranial pressure and mean arterial blood pressure. Dev. Brain Res. 95 (2), 272–282. [PubMed: 8874903]

Rěhulka P, Cimbálník J, Pail M, Chrastina J, Hermanová M, Brázdil M, 2019. Hippocampal high frequency oscillations in unilateral and bilateral mesial temporal lobe epilepsy. Clin. Neurophysiol. 130 (7), 1151–1159. [PubMed: 31100580]

Reid AY, Bragin A, Giza CC, Staba RJ, Engel J, 2016. The progression of electrophysiologic abnormalities during epileptogenesis after experimental traumatic brain injury. Epilepsia. 57 (10), 1558–1567. [PubMed: 27495360]

Sheybani L, Birot G, Contestabile A, Seeck M, Kiss JZ, Schaller K, et al. , 2018. Electrophysiological evidence for the development of a self-sustained large-scale epileptic network in the Kainate mouse model of temporal lobe epilepsy. J. Neurosci. 38 (15), 3776–3791. [PubMed: 29555850]

Smith SM, 2002. Fast robust automated brain extraction. Hum. Brain Mapp. 17 (3), 143–155. [PubMed: 12391568]

Staba RJ, Wilson CL, Bragin A, Fried I, Engel J Jr., 2002. Quantitative analysis of high-frequency oscillations (80–500 Hz) recorded in human epileptic hippocampus and entorhinal cortex. J. Neurophysiol. 88 (4), 1743–1752. [PubMed: 12364503]

Turtzo LC, Budde MD, Gold EM, Lewis BK, Janes L, Yarnell A, et al. , 2013. The evolution of traumatic brain injury in a rat focal contusion model. NMR Biomed. 26 (4), 468–479. [PubMed: 23225324]

Waldman ZJ, Shimamoto S, Song I, Orosz I, Bragin A, Fried I, et al. , 2018. A method for the topographical identification and quantification of high frequency oscillations in intracranial electroencephalography recordings. Clin. Neurophysiol. 129 (1), 308–318. [PubMed: 29122445]

Worrell GA, Parish L, Cranstoun SD, Jonas R, Baltuch G, Litt B, 2004. High-frequency oscillations and seizure generation in neocortical epilepsy. Brain. 127 (7), 1496–1506. [PubMed: 15155522]

Wu JY, Sankar R, Lerner JT, Matsumoto JH, Vinters HV, Mathern GW, 2010. Removing interictal fast ripples on electrocorticography linked with seizure freedom in children. Neurology. 75 (19), 1686–1694. [PubMed: 20926787]

Yung Y-F, Bentler PM, 1996. Bootstrapping techniques in analysis of mean and covariance structures. In: Advanced Structural Equation Modeling: Issues and Techniques, pp. 195–226.

Zhang Y, Brady M, Smith S, 2001. Segmentation of brain MR images through a hidden Markov random field model and the expectation-maximization algorithm. IEEE Trans. Med. Imaging 20 (1), 45–57. [PubMed: 11293691]

Zijlmans M, Jiruska P, Zelmann R, Leijten FSS, Jefferys JGR, Gotman J, 2012. High-frequency oscillations as a new biomarker in epilepsy. Ann. Neurol. 71 (2), 169–178. [PubMed: 22367988]

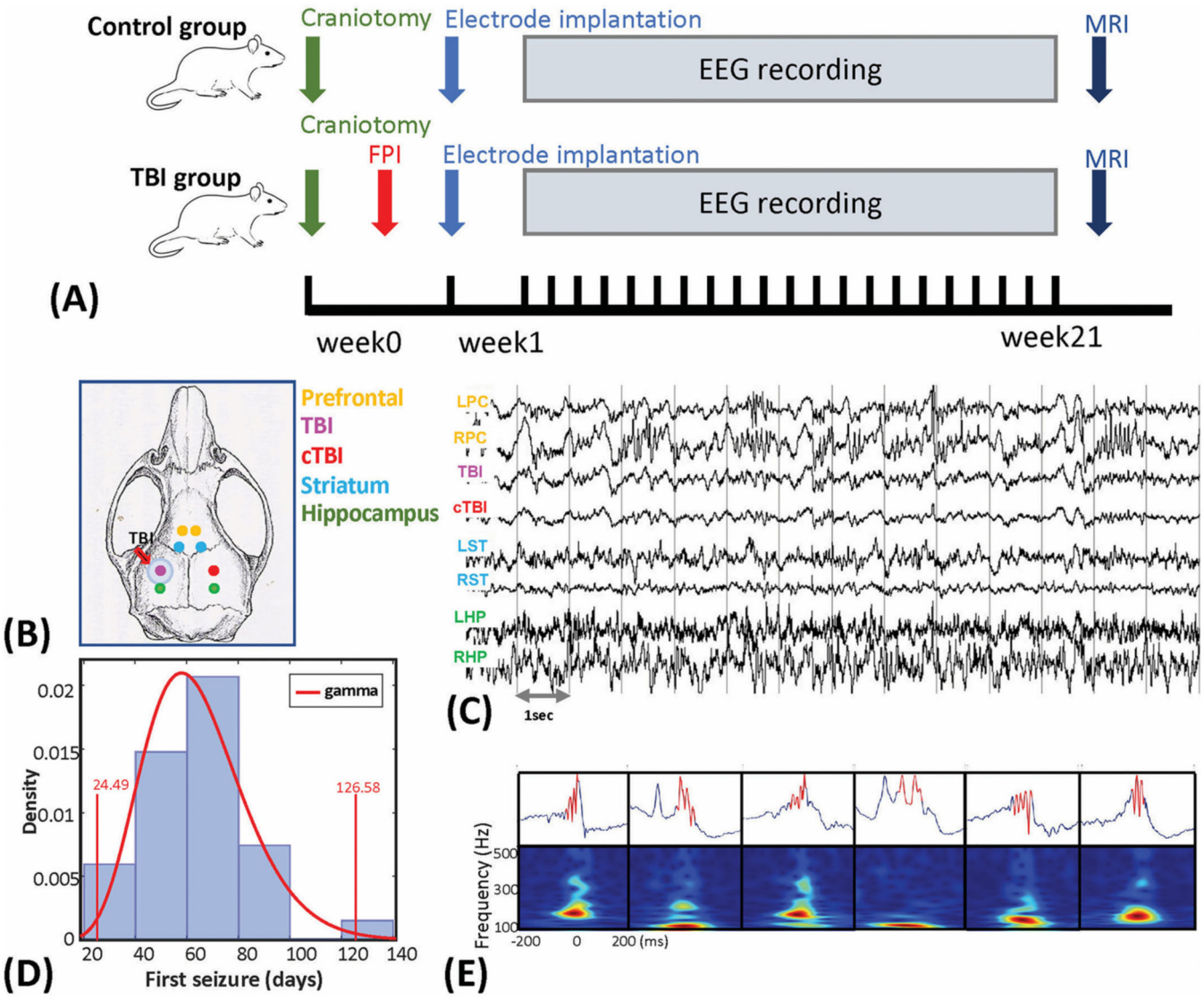

Fig. 1.

Schematic diagram of depth electrode recordings, first seizure onset, and demonstration of HFOs. (A) The experimental design and protocols for this study. (B) Electrode implantation sites superimposed on the rat skull. Electrodes were implanted bilaterally in the prefrontal cortex (PFC), peri-lesion area and homotopic contralateral cortex, striatum, and hippocampus. (C) Unfiltered segment of local field potentials (LFPs) from the eight recording sites. Abbreviations: L and R – left and right; PC – prefrontal cortex; TBI – traumatic brain injury area; cTBI – contralateral to the TBI area; ST – striatum; HP – hippocampus. (D) Histogram of the first spontaneous seizure onset (in days). The distribution fitting analysis were performed and the gamma distribution was chosen as the best fitting distribution of the data. Vertical line at 24.49 days and 126.58 days indicates the upper and lower boundaries of the 1% significance level for the test statistics with the fitted gamma distribution. (E) Demonstration of the detected HFO events from the CA1 area of hippocampus. Automatic HFO detection and refinement algorithm was applied, details were

described in Supplementary S1. The upper plots showed the unfiltered LFPs and bottom plots were the time-frequency plot between 100 and 500 Hz in a range of 400 ms (centered with the peak of HFOs).

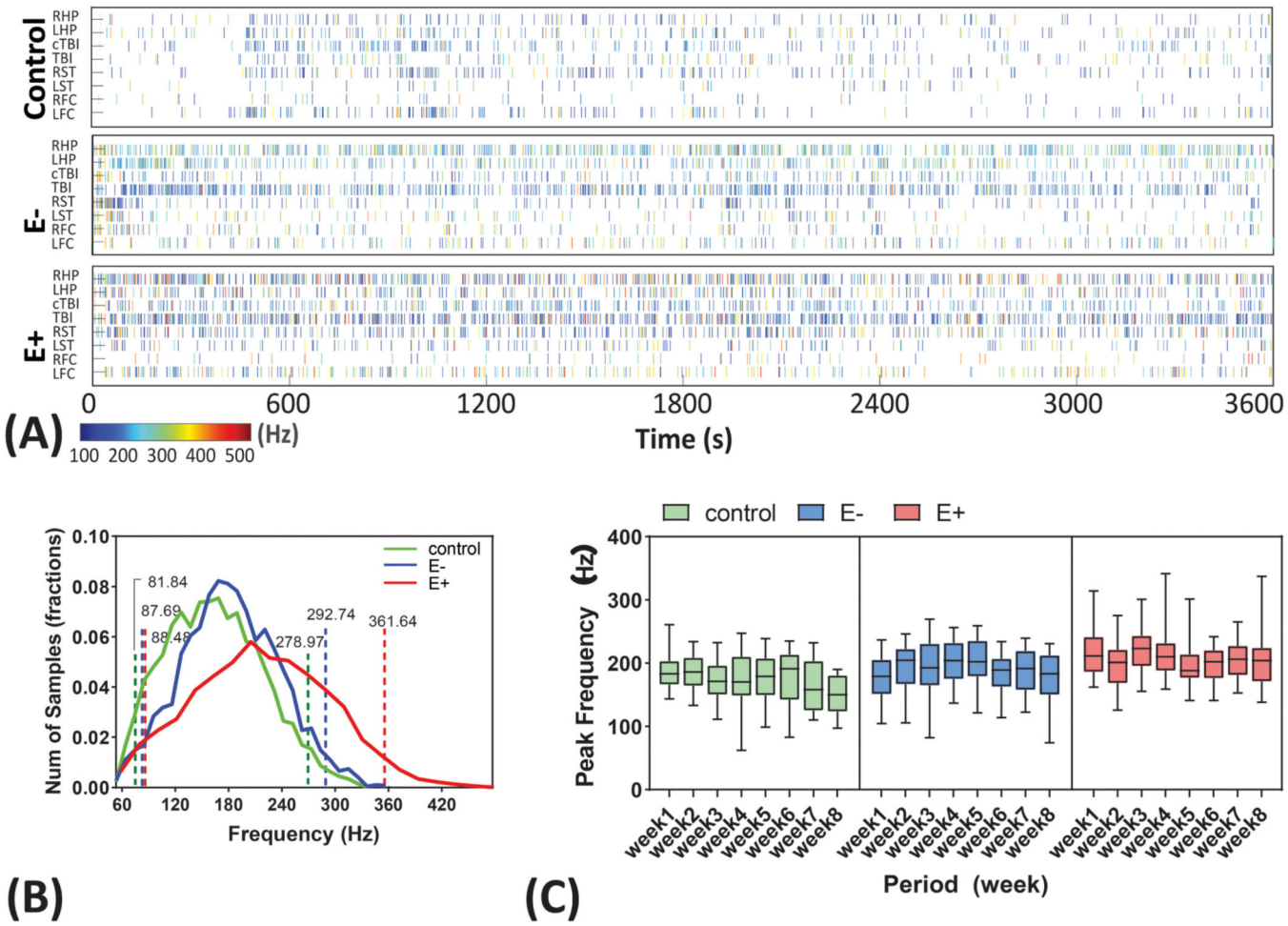

Fig. 2.

Peak frequency distributions and consistency. (A) HFO events presented in a selected 1-hour file from control, E− and E+ group in the 8 brain recording sites. Each bin represents a HFO events with the color indicates the peak frequency (blue- low, red- high). Abbreviations are similar to those in the Fig. 1). (B) HFO peak frequency distribution in control, E− and E+ group. The range of HFO was plotted between 60 and 480 Hz. Control, E− and E+ group showed a mean peak frequency of 170.9, 190.2 and 219.1 Hz. Dashed lines represent the 95% confidence of interval of the mean. E+ group were found significantly larger than E− and control group at the alpha = 0.05. No differences were found between control and E− group. (C) Consistency of the HFO peak frequency presented as group × weeks. No within-group differences were found for all three group in the 8-week test period. (For interpretation of the references to color in this figure legend, the reader is referred to the web version of this article.)

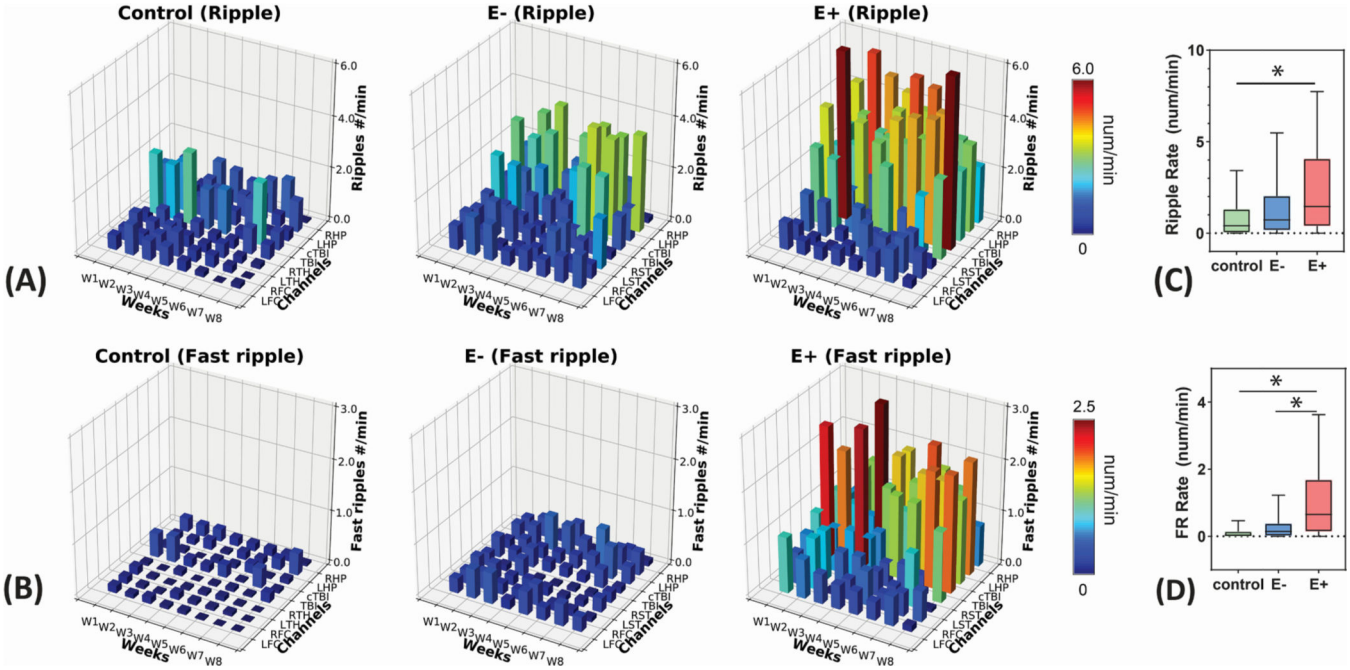

Fig. 3.

Spatial and temporal distributions of HFOs. (A) 3D bar plots of brain region × week HFO distribution for Ripples and (B) Fast Ripple events. Data were presented in the total of 203,550 HFOs, including 150,874 Ripples and 52,676 Fast Ripples. The different colors indicate the rate of Ripples and Fast Ripples. (C) Comparison of total Ripple rate and (D) Fast Ripple rate among three groups. *: $p < 0.05$.

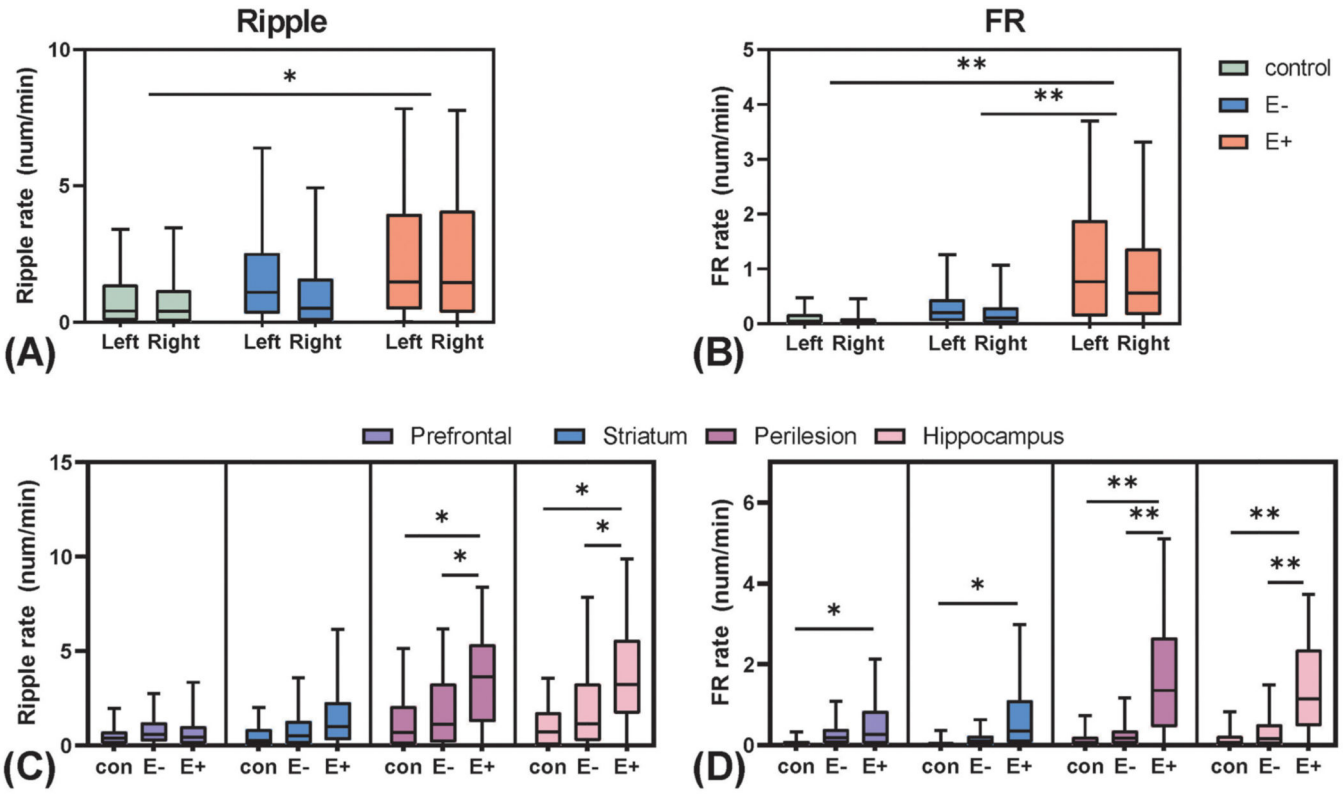

Fig. 4.

Analysis of spatial distribution of Ripples and Fast Ripples in control, E− and E+ groups. Within- and between-group comparison of Ripple (A) and Fast Ripple events in response to ipsilateral and contralateral hemispheres. No within-group differences were found between ipsilateral and contralateral HFO rates, while significant larger Ripple and Faster Ripple rates were observed in the E+ group in both side of the brain in comparison of other groups. Between-group comparison of Ripple and (D) Fast Ripple rates in four brain regions (prefrontal, striatum, perilesional, and hippocampus). The Ripple and Fast Ripple rates in E+ group in the perilesional site and hippocampus were significantly larger than other two groups while FRs also larger in prefrontal cortex and striatum for E+ vs control. *: $p < 0.05$. ** $p < 0.001$.

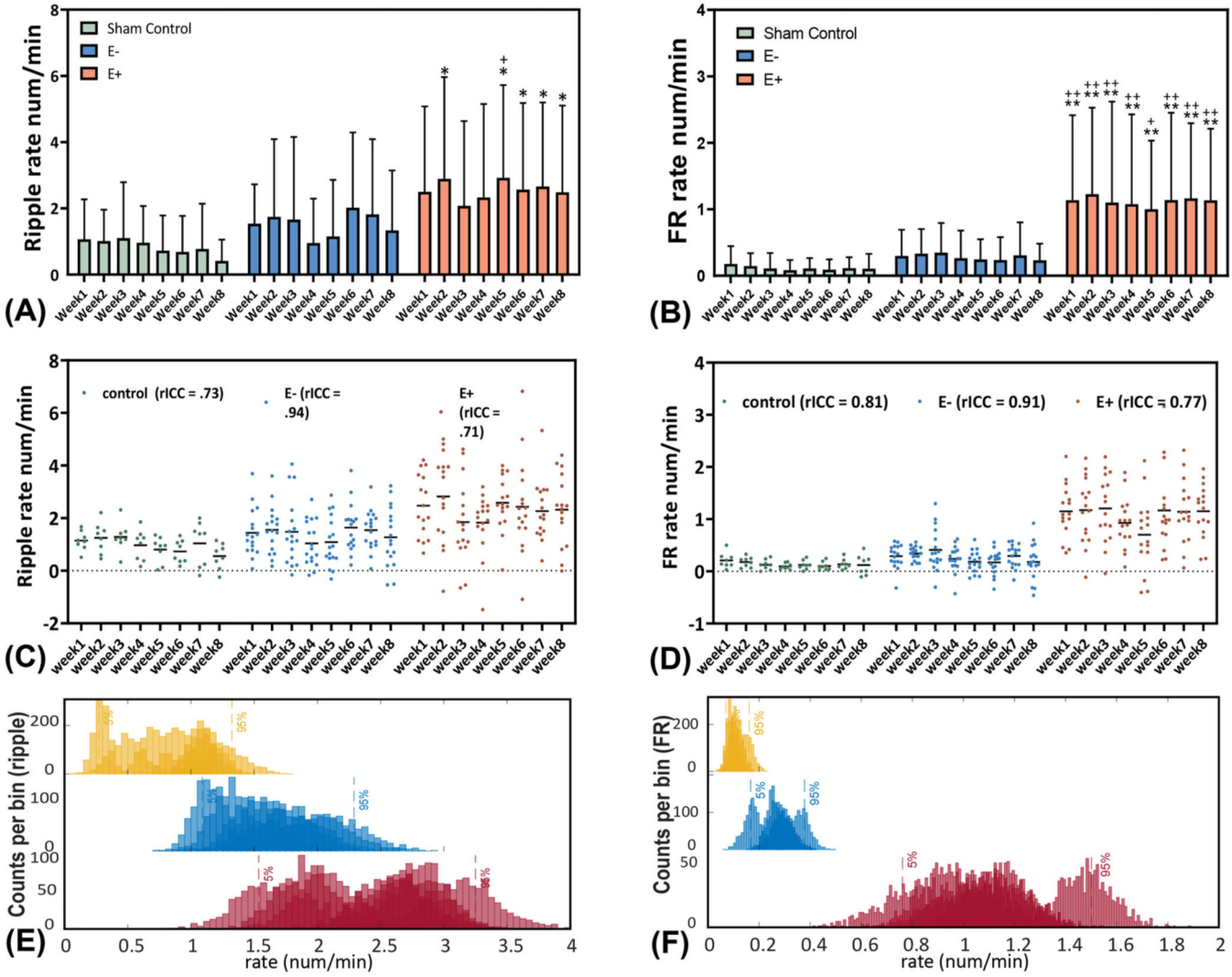

Fig. 5.

The temporal occurrences of HFOs during PTE. The occurrence rates of (A) Ripples and (B) FRs in three groups. Data were analyzed from the week1 – week 8 after TBI. (C & D) The temporal stability evaluated by the corrected intraclass correlation coefficient (rICC). Control group and E+ group showed the moderate reliability and E− group showed an excellent reliability in their weekly ripple rates. In addition, control group and E+ group showed a good reliability while E− group showed an excellent reliability in the weekly fast ripple rate. The evaluation criteria were followed by (Koo and Li, 2016): a ICC value <0.5 are indicative of poor reliability, value between 0.5 and 0.75 indicate moderate reliability, values between 0.75 and 0.9 indicate good reliability, and values greater than 0.90 indicate excellent reliability. (E & F) The stacked weekly Ripple and Fast Ripple bootstrapping distributions (surrogates = 1000) of Ripple and FR occurrences (num/min) within each group. Overlapped distributions and the 95%CI indicated a consistency of temporal occurrences of HFO rates in all groups. * & **: E+ vs. control group, $p < 0.05$, $p < 0.001$. + & ++: E+ vs. E− group, $p < 0.05$, $p < 0.001$.

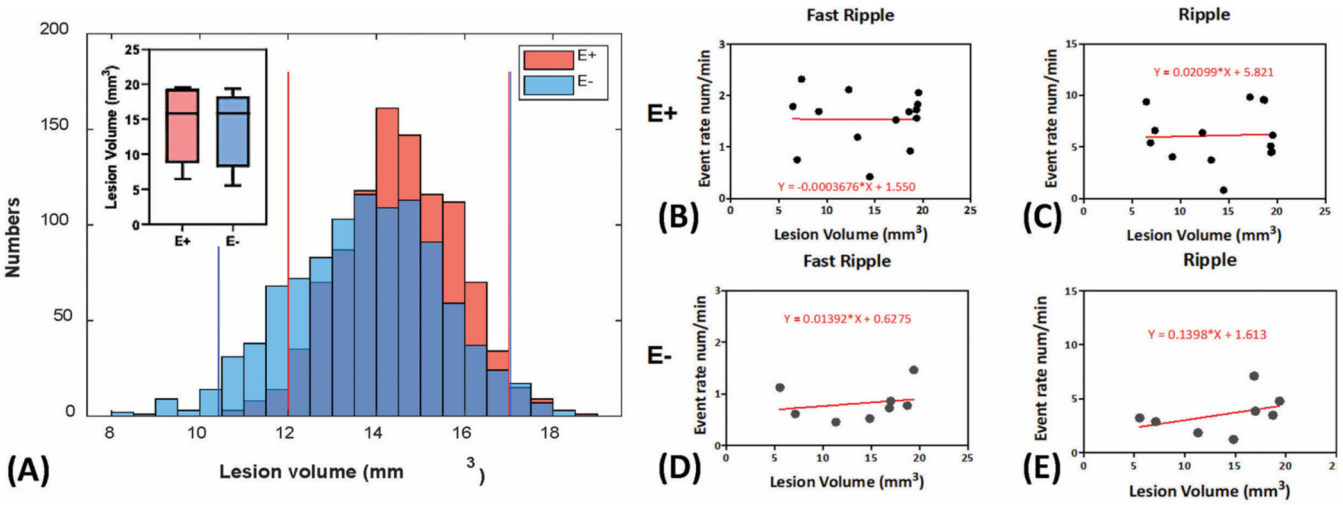

Fig. 6.

Relationship of lesion size and the occurrence of HFO. (A) Comparison of lesion volume (mm^3) between E− and E+ group. A permutation approach (surrogates = 1000) was applied to estimate the result reliability. No group differences were obtained under the 95%CI. (B-E) The linear regression analysis of the Ripple and Fast Ripple rates with the lesion volumes within E+ and E− group. No significant linear relationship was found. * & **: E+ vs. control group, $p < 0.05$, $p < 0.001$. + & ++: E+ vs. E− group $p < 0.05$, $p < 0.001$.

Table 1

Descriptive statistics of HFO occurrence rates (num/min) in control, E− and E+ group.

Event type		Sham (n = 8)	E− (n = 18)	E+ (n = 22)
HFO	Total numbers	16,858	53,622	133,070
	Mean (SD)	1.00 (1.32)	1.81 (2.21)	3.64 (3.48)
	Range (min, max)	(0, 9.07)	(0, 14.46)	(0,14.68)
Ripple	Total numbers	14,895	44,755	91,224
	Mean (SD)	0.88 (1.23)	1.53 (2.04)	2.52 (2.67)
	Range (min, max)	(0, 9.05)	(0, 14.03)	(0, 14.22)
Fast ripple	Total numbers	1963	8867	41,846
	Mean (SD)	0.11 (0.19)	0.28 (0.38)	1.11 (1.2784)
	Range (min, max)	(0, 1.42)	(0, 2.34)	(0, 6.9513)